Journal of Materials Chemistry A

Accepted Manuscript

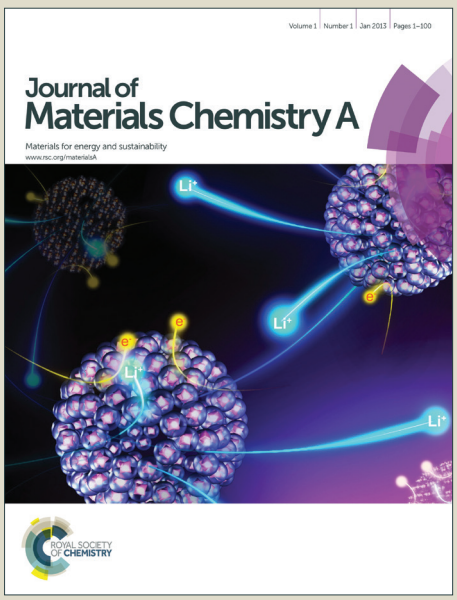

This is an *Accepted Manuscript*, which has been through the Royal Society of Chemistry peer review process and has been accepted for publication.

Accepted Manuscripts are published online shortly after acceptance, before technical editing, formatting and proof reading. Using this free service, authors can make their results available to the community, in citable form, before we publish the edited article. We will replace this *Accepted Manuscript* with the edited and formatted *Advance Article* as soon as it is available.

You can find more information about *Accepted Manuscripts* in the Information for Authors.

Please note that technical editing may introduce minor changes to the text and/or graphics, which may alter content. The journal's standard Terms & Conditions and the Ethical guidelines still apply. In no event shall the Royal Society of Chemistry be held responsible for any errors or omissions in this *Accepted Manuscript* or any consequences arising from the use of any information it contains.

ROYAL SOCIETY OF CHEMISTRY

www.rsc.org/materialsA

Cite this: DOI: 10.1039/c0xx00000x

www.rsc.org/xxxxxx

ARTICLE TYPE

A facile synthesis for hierarchical porous CeO_2 nanobundles and their superior catalytic performance for CO oxidation

Richuan Rao,*[a] Ming Yang,[b] Changshun Li,[b] Huaze Dong,[a] Song Fang[a] and Aimin Zhang*[b]

Received (in XXX, XXX) Xth XXXXXXXXX 20XX, Accepted Xth XXXXXXXXX 20XX

DOI: 10.1039/b000000x

In this study, we develop a facile hydrothermal route to build a nanostructure of porous CeO_2 nanobundles with hierarchical architectures by the design and growth of anisotropic CeO_2 precursors in a carbonate-assisted formaldehyde hydrothermal system without templates and surfactants. The synthetic key is to control the formation of their anisotropic CeO_2 precursors with formate and carbonate promoted by carbonate and ammonium ions during the employed hydrothermal treatment. The as-prepared CeO_2 nanobundles have a hierarchical porous structure assembled by numerous nanorods with small diameter and show much higher catalytic activities for CO oxidation compared with CeO_2 nanorods, nanowires and nanoparticles prepared by formaldehyde-assisted hydrothermal treatment and traditional precipitation methods. The outstanding catalytic performance for the nanobundles is attributed to their excellent physicochemical properties, such as larger lattice cell parameters, much larger surface areas and the best redox behaviour of surface oxygen on CeO_2 surface.

1. Introduction

As one of promising nanomaterials, hierarchical nanomaterials built with low dimensional nanostructures has attracted intensive research interests due to remarkable properties and promising applications in heteocatalysis, biotechnology, electronics, optics.[1-4] Stimulated by their unique structure and fantastic properties, many efforts have been focused on the fabrication of nanomaterials with the hierarchical nanoarchitecture.[3-6] At present, some efficient strategies have been developed to fabricate the hierarchical nanostructured materials by self-assembly of primary nanocrystals,[7-9] Kirkendall process[10,11] and template precursors.[12-14] Although great progress has been achieved on the synthesis approaches for these nanomaterials with hierarchical architectures, it is usually necessary to present surfactants or templates and a series of complicated procedures during their synthetic processes, leading to be energy-consuming, high cost and manufacture-complicated. In addition, the porous structure is largely introduced to extend the potential applications of the unique nanomaterials, such as catalytic chemistry, bioengineering, environmental protection, sensors, and other fields.[15-17] Therefore, it is still of fundamental significance to develop facile, mild and efficient approaches for the large-scale synthesis of novel hierarchical nanostructured materials with porous structure from independent and discrete nanoscale building blocks.

As one of the most important rare earth oxides, CeO_2 with unique properties has attracted much attention in recent years due to their exceptional technological applications in oxygen storage capacity, high thermal stability, optical properties, and electrical conductivity and diffusivity.[18,19] Recent advances in morphology-controlled synthesis of the nanomaterials offer new opportunities of developing novel CeO_2 functional materials with desired structural properties. It has been reported that numerous morphologies of cerium oxides, such as nanorods,[20,21] nanowires,[22,23] nanotubes,[24,25] nanobelts[26,27] and other morphologies,[28-34] are synthesized by chemical and physical methods. The nanomaterials with these morphologies show their positive properties and their potential applications. Usually, most of the synthetic systems for these CeO_2 nanomaterials employ aqueous solution routes which are feasible, low-cost, simply operated and easily industrialized for the fabrication of nanoscale metal oxide materials. Since CeO_2 with the cubic structure has no intrinsic driving force for anisotropic growth in aqueous routes, numerous CeO_2 nanomaterials with various morphologies are indirectly synthesized by the help of controlling their corresponding template precursors with anisotropic structure, e.g. $Ce(OH)_3$,[20,21] $Ce(HCOO)_3$,[28] $Ce(OH)CO_3$,[29,30] $Ce_2(C_2O_4)_3$.[31,32] Although hierarchical CeO_2 materials with nanorod structure have been prepared by phosphate-assisted hydrothermal routes, occlusion electrodeposition approaches and microwave-assisted precipitation methods,[35-37] the great majority of these discovered template precursors with anisotropic structure are very difficultly used directly to prepare hierarchical CeO_2 nanomaterials. The general strategies are that various types of surfactants or templates have widely been used in most solution routes for the synthesis of well structured materials with hierarchical architectures. However, these synthetic processes usually result in higher synthesis cost, larger energy consumption and more complicated manufacture procedures. Therefore, the fabrication of CeO_2 hierarchical architectures based on low dimensional building blocks still remains a challenge.

Journal of Materials Chemistry A Accepted Manuscript

Here, we describe a facile, mild and low-cost hydrothermal route to synthesize hierarchical and porous CeO_2 nanostructured materials to design and grow anisotropic CeO_2 precursors in a carbonate-assisted formaldehyde hydrothermal system without templates and surfactants. It is found that the synthetic key for the CeO_2 hierarchical architectures is to control the formation of the precursor products with formate and carbonate promoted by ammonium ions and carbonate during the hydrothermal treatment. After calcination, the as-prepared CeO_2 nanobundles are porous hierarchical materials with microporous and mesoporous structure, exhibit very larger surface area ($130.4 m^2 g^{-1}$) and enhance catalytic performance for CO oxidation, compared to CeO_2 nanorods, nanowires and nanoparticles prepared by other synthetic methods. In addition, the carbonate-assisted formaldehyde hydrothermal route in the presence of ammonium salts may open a new insight into fabricating rare earth oxides with hierarchical architectures built by low dimensional structure and extending potential applications of CeO_2 materials.

2. Experimental

2.1 Materials

Cerium(III) nitrate hexahydrate (purity ≥99.0%) was provided by Sinopharm chemical reagent Co. Ltd. Formalin solution (purity 37.0-40.0%), ammonia (purity 25.0-28.0%), sodium hydroxide (purity >96%), potassium hydroxide (purity >86%) and ammonium bicarbonate (purity 21.0-22.0 NH_3%) was purchased from Nanjing Chemical Reagent Co. Ltd. All the reagents were used as received.

2.2 Synthesis of CeO_2 nanobundles

In a typical hydrothermal synthesis process, 1.0 g of cerium (III) nitrate hexahydrate was dissolved in 17.5ml formalin aqueous solution at room temperature, 2.5ml ammonia was slowly mixed to the solution and then 1g ammonium bicarbonate was slowly added to the mixed solution under vigorous stirring. The suspending solution was immediately transferred into a 50 ml Teflon-lined stainless autoclave and heated at 60°C for 20h, followed by naturally cooling to room temperature. The precipitates were filtered, washed and dried at 60°C overnight. The resulting powders were heated to 450°C in air at a rate of 2°C min^{-1} and calcined for 5h. The light yellow samples of CeO_2 nanobundles were obtained.

CeO_2 nanorods and nanowires were prepared by a hydrothermal method and used as comparison reference samples.[26] Typically, 1.0g of cerium(III) nitrate hexahydrate was dissolved in 30 ml formalin solution and then 1.0 or 2.1g of sodium hydroxide or potassium hydroxide was slowly added to mixed solution under vigorous stirring. Then, the suspended solution was transferred into a 40 ml Teflon-lined stainless autoclave and heated at 120 or 100°C for 20 h in an electric oven. Subsequently, the same procedures with the preparation of CeO_2 nanobundles were applied. The resulting samples of CeO_2 nanorods or nanowires were obtained.

CeO_2 nanoparticles were prepared by a traditional precipitation method reported in the literature.[20] $Ce(NO_3)_3 \cdot 6H_2O$ was dissolved in deionized water and the pH value of the solution was rapidly adjusted to 12 by adding NaOH solution with stirring. Then the precipitates were filtrated, washed with deionized water, dried at 60°C for 24 h and calcined at 450°C for 5 h.

2.3 Characterization

Scanning electron microscopy (SEM) measurements were performed on Hitachi S4800 instrument. Transmission electron microscopy (TEM) observations were carried out by JEOL-JEM-1005 transmission electron microscope at 200kV. Powder XRD measurements were performed on Philips X'pert Pro X-ray diffractometer with Cu Kα radiation and operated at 40kV and 40mA. N_2 adsorption-desorption isotherms were measured at 77K, using Micromeritics ASAP 2000 equipment. The Brunauer-Emmet-Teller (BET) methods and Barrett-Joyner-Halenda (BJH) models were used for surface area calculation and porosity evaluation, respectively. Ultraviolet-visible (UV-vis) diffuse reflectance spectra were performed under ambient conditions using a Shimadzu UV3600 spectrophotometer equipped with an integrating sphere. $BaSO_4$ was used as a reference and the spectra were recorded in the range of 200-800 nm. FT-IR spectra were recorded on Bruker Vector 22 at a resolution of $4 cm^{-1}$ in KBr tablets. The reducibility of samples was studied by H_2-TPR in a mixture flow of 5 vol.% H_2 in N_2, using a flow system equipped with a TCD detector. The temperature change was from room temperature to 800 ◦C at a rate of 10 ◦C min^{-1}.

2.4 Catalysis tests

The catalytic activities for CO oxidation were carried out in a conventional fixed-bed quartz microreactor (8mm in outer diameter) under ambient pressure. 30mg catalyst was placed in the quartz microreactor in each run. The system was first purged with high-purity N_2 gas ($40 ml min^{-1}$) at 100°C for 60min, cooled to room temperature. Then the reactant gases, which were mixed with pure O_2 and 5% CO balanced by nitrogen(CO/O_2 volume ratio=0.15), were fed into the reactor at a rate of $40 ml min^{-1}$ and have a gas hourly space velocity (GHSV) of 80,000 $ml \cdot h^{-1} \cdot g^{-1}$. The reaction products were analyzed by gas chromatography (SP-2100) with TCD and the column packed 13X molecular sieve.

3. Results and discussion

Since CeO_2 with the cubic structure does not grow anisotropically due to any intrinsic driving force in aqueous routes, CeO_2 nanobundles with hierarchical architectures are indirectly synthesized by controlling the growth of CeO_2 precursors with anisotropic structure in a carbonate-assisted hydrothermal system in the presence of formaldehyde without templates and surfactants. When cerium salts are firstly mixed with formalin solution, the mixed solution has the brown colour without any precipitation in spite of the usage of ammonia solution. If ammonium bicarbonate is added into the mixed solution, the white colloidal precipitates with amorphous morphology are immediately produced in the brown solution. The colloidal precipitates can be dissolved by hydrochloric acid and accompanied by gas evolution, indicating that they are composed of carbonate with cerium element. During hydrothermal treatment, formaldehyde from the synthesized system is converted into formate by Cannizzaro disproportionation reaction.[26,38] Subsequently, the produced formate attacks the colloidal

Journal of Materials Chemistry A Accepted Manuscript

This journal is © The Royal Society of Chemistry [year]

precipitates with carbonate to result in their hydrolysis and then these ions renucleates to grow anisotropically into the CeO_2 nanobundle precursors. Based upon the above observations, it is believed that the CeO_2 nanobundle precursors are formed at low hydrothermal temperatrue via a dissolution-reprecipitation mechanism in carbonate-assisted hydrothermal conditions in the presence of formaldehyde.[39,40]

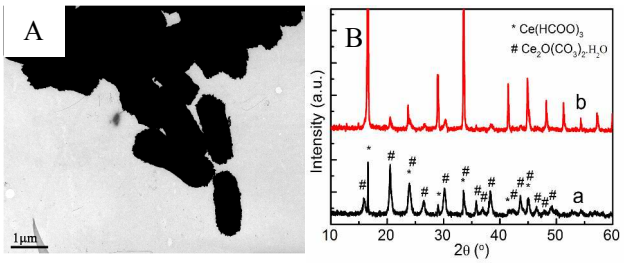

Fig.1 (A) TEM image of CeO_2 nanobundle precursors, (B) XRD spectra. (a) Nanobundles, (b) Cerium formate.

Fig.1A exhibits the TEM image of the as-prepared CeO_2 precursors with nanobundle structure. The XRD patterns in Fig.1B (Line a) reveal that the characteristic peaks of the nanobundle precursors can readily be indexed to $Ce(HCOO)_3$ (JCPDS 80-1503) and $Ce_2O(CO_3)_2 \cdot H_2O$ (JCPDS 44-0617), indicating that formate and carbonate are truly presented in the CeO_2 precursors. FT-IR spectra in Fig.S1 (Line a) further show that the absorption peaks in the ranges of 1520 to 1430cm^{-1}, 1089 to 1080cm^{-1}, 885 to 850cm^{-1} and 750 to 660cm^{-1} can be assigned to the vibration mode of carbonate.[26,38,41] Moreover, the absorption peaks in the range of 2700-3000cm^{-1} corresponding to the stretching peaks of C-H bands, the absorption peaks between 1350 and 1600cm^{-1} and the fingerprint peak at 775 cm^{-1} are similar with the absorption peaks of formate in the line b of Fig.S1, which reveals the presence of formate.[26,28,38] It is also seen that there is the Ce-O stretching band at about 400cm^{-1} for the nanobundle precursors. These characterization results indicate that there are mainly cerium, carbonate and formate in the CeO_2 nanobundle precursors.

It is noteworthy that ammonium ions and carbonate play significant roles in the formation of the anisotropic CeO_2 nanobundle precursors with formate and carbonate in the formaldehyde-assisted hydrothermal system. A series of control experiments are used to reveal effect of carbonate and ammonium ions on morphology of CeO_2 nanobundle precursors. If carbonate is not used in the synthetic system, the prepared samples take on the nanorod structure as shown in Fig.S2 and the XRD pattern in the line b of Fig.1B indicates that the characteristic peaks of the precursor samples can readily be indexed to the hexagonal and rhomb-centered structure of $Ce(HCOO)_3$ (JCPDS 80-1503). When carbonate is added into the synthetic hydrothermal system, CeO_2 nanobundle precursors are obtained after the hydrothermal treatment as shown in Fig.1A. On the other hand, NH_4^+ ions exist simultaneously in the formaldehyde hydrothermal system with carbonate and play an important role in the growth of the nanobundle precursors. If sodium ions are dominant to substitute ammonium ions in the employed hydrothermal system, the as-obtained products only possess the nanorod structure with 100-300nm in diameter and several micrometers in length as shown in Fig.S3A and while the dominant potassium ions in the hydrothermal system result in the cerium precursors with unpredictable or undesired morphology as shown in Fig.S3B. In addition, these cerium precursor samples are clearly observed to have poor degree of crystallinity from the TEM image in Fig.S3A and B. Evidently, carbonate and ammonium ions can promote the production of CeO_2 nanobundle precursors with carbonate and formate in the formaldehyde-assisted hydrothermal system.

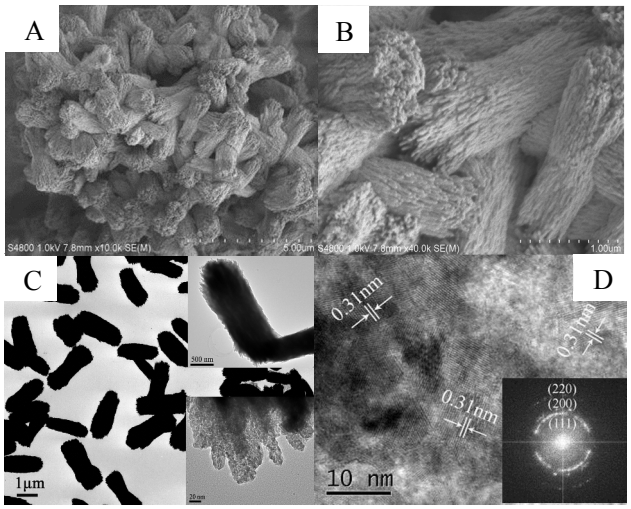

Fig.2 (A, B) SEM images, (C) TEM images, the insert are TEM images of single nanobundle (upper right) and its tip (lower right), (D) High-resolution TEM images of CeO_2 nanobundles, the insert is FFT image of CeO_2 nanobundles.

Fig.2 shows typical SEM and TEM images of CeO_2 nanobundles by calcining their corresponding precursors from the carbonate-assisted hydrothermal systems with formaldehyde. The SEM image in Fig.2A shows that the as-synthesized CeO_2 nanobundles are typically of 0.5-1.2μm in width and 2-4μm in length. Each nanobundle is assembled by numerous nanorods with less than 30nm in diameter as shown in Fig.2B, indicating the hierarchical structure of CeO_2 nanobundles assembled with low dimensional nanorods. From the TEM images in Fig.2C, CeO_2 nanobundles take on the feature of porous structure, indicating porous CeO_2 materials. The high-resolution TEM image of Fig.2D reveals that CeO_2 nanobundles clearly show the secondary structure by the agglomeration of each primary particle with 5-10nm grain size. The corresponding fast Fourier transform (FFT) image in the inset of Fig.2D reveals that these primary particles possess the mainly exposed planes [111] with the interplanar spacing 0.31nm. As comparison samples, Fig.S4 shows TEM images of CeO_2 nanorods, nanowires and nanoparticles prepared successfully by formaldehyde-assissted hydrothermal treatment and traditional precipitation methods. The high-resolution TEM images confirm that these nanostructure CeO_2 samples mainly expose the [111] crystal planes with the interplanar spacing 0.31nm.

Journal of Materials Chemistry A Accepted Manuscript

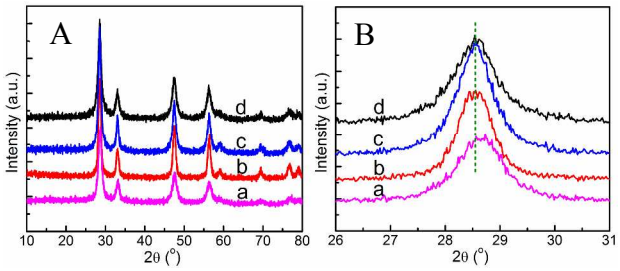

Fig.3 (A) XRD spectra, (A) XRD spectra (2θ=26°-31°) of CeO_2 samples. (a) Nanowires, (b) Nanoparticles, (c) Nanorods, (d) Nanobundles.

Phases and purities of the as-synthesized CeO_2 nanostructure materials are investigated by the XRD analysis. Fig.3A shows the XRD patterns of CeO_2 nanobundles. The characteristic peaks of the CeO_2 materials can readily be indexed to pure cubic fluorite structure CeO_2 (JCPDS 34-0394) and no signal of impurities is detected, indicating that the CeO_2 nanocrystals with high purity can be obtained under the current synthetic system. To reveal the structure difference between CeO_2 nanobundles and other nanostructure CeO_2 samples, the diffraction peaks [111] at about 28.5° are investigated in Fig.3B. The shift of the main diffraction peak for the nanobundles is hardly observed relative to nanorods and nanoparticles, but the shift is obviously observed in comparison with CeO_2 nanowires, indicating that CeO_2 nanobundles possess larger lattice cell parameters and lattice cell expansion than CeO_2 nanowires and it is the same with CeO_2 nanorods and nanoparticles as shown in Table S1. Furthermore, the full width at half maximum from [111] diffraction peak is measured to calculate the mean grain size of CeO_2 nanobundles according to Scherrer's equation ($D = 0.89\lambda/\beta\cos\theta$, where D is grain size, λ is the X-ray's wavelength, β is the FWHM of the peak, and θ is Bragg's angle) and the calculated results are listed in Table S1. It is found that the nanobundles have larger mean grain size of primary particles than nanowires, yet smaller than nanorods and nanoparticles.

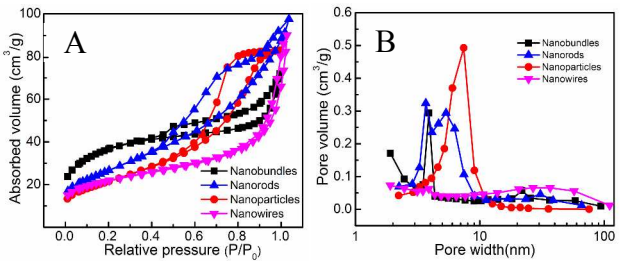

Fig.4 (A) N_2 adsorption-desorption isotherms; (B) pore size distribution curves of CeO_2 samples.

The textural properties of the as-obtained CeO_2 nanobundles are investigated with the nitrogen adsorption-desorption isotherms as shown in Fig.4. For CeO_2 nanobundles, the pronounced hysteresis loops in the isotherm curves are observed in Fig.4A and the isotherm can readily be ascribed to a typical type IV isotherm according to the IUPAC classification,[42] indicating the presence of mesopores. It is also noticed that the adsorption branch of CeO_2 nanobundles is similar with type I isotherm curves and there is a greater adsorption capacity in the low relative pressure (P/P_0), indicating the presence of micropores. The BJH pore size distributions from desorption branch in Fig.4B also show that the nanobundles possess the mesopore structure with 4.1nm pore size and the other micropore structure below 2nm pore size. Furthermore, CeO_2 nanorods show a type IV isotherm with hysteresis loops indicating the presence of mesopore, CeO_2 nanoparticles display a type IV isotherm with the hysteresis loops at high relative pressure (P/P_0) associated with aggregates of CeO_2 particles giving rise to slitlike pores, and CeO_2 nanowires take on the type I isotherm characteristic of microporous structure.[42] The BET measurement indicates that the nanobundles with unique porous structure possess the largest surface area with 130.4m^2g^{-1} as shown in Table S1.

H_2-TPR experiments are used to detect the redox properties of CeO_2 materials. Fig.S5 displays H_2-TPR profiles of these CeO_2 samples. We can observe a broad reduction peak (350-600°C) from the reduction of surface ceria or reduction of surface oxygen species.[19] It is also found that CeO_2 nanobundles have the lower initial reduction temperature and the earlier emerged reduction peak profiles than CeO_2 nanowires. Besides, although CeO_2 nanobundles have similar initial reduction temperature with nanorods and nanoparticles, their different peak profiles reveal different reduction behaviour among them. Due to the asymmetry of these reduced peaks, they can be divided into two peaks, a peak at 350-500°C and the other peak at 500-600°C as shown in Fig.S5.[43] It is further found that CeO_2 nanobundles have the similar position of the reduced peak at 350-500°C with nanorods and nanoparticles, but show lower temperature of the reduction peak at 500-600°C. Furthermore, since the amount of H_2 consumption is in direct proportion to the peak area of the TPR curve for CeO_2 samples, the CeO_2 nanobundles exhibit the largest peak area in TPR profiles and the highest amount of H_2 consumption. Therefore, CeO_2 nanobundles are more easily reduced to provide surface oxygen species and promote oxygen mobility on their surface.

The absorption properties for the as-prepared ceria nanobundles are investigated by UV-vis absorption spectroscopy as shown in Fig.5A. The nanobundle samples (line a) show the typical absorption spectra of CeO_2 and the positions of their absorption peaks are nearly consistent with other CeO_2 samples. The strong absorption below 400nm is observed in the UV region, which can be attributed to the charge-transfer transition from O2p to Ce4f and block damage by UV radiation.[44] However, the nanobundles have a different absorption edge from other CeO_2 samples and their energy band gaps are further calculated in order to clarify the difference of the absorption properties for those CeO_2 samples.

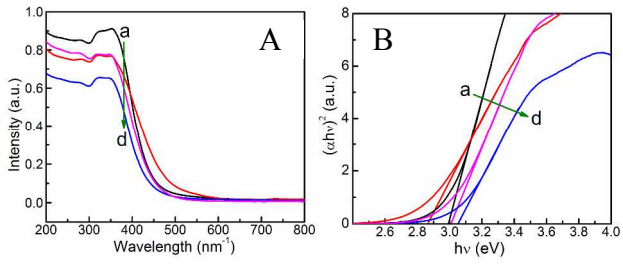

Fig.5 (A) UV absorption spectra; (B) plots of $(\alpha h\nu)^2$ versus photon energy for CeO_2 materials. (a) Nanobundles, (b) Nanoparticles, (c)

Journal of Materials Chemistry A Accepted Manuscript

This journal is © The Royal Society of Chemistry [year]

Nanowires, (d) Nanorods.

The energy band gap of CeO_2 samples can be calculated from the equation:

$$\alpha \propto (h\nu - E_g)^{1/2}/h\nu$$

where α is the absorption coefficient, E_g is the band gap energy for direct transitions.[45] The plots of $(\alpha h\nu)^2$ vs hν are shown in Fig.5B. The E_g values (2.99eV) of the CeO_2 nanobundles are estimated to be smaller than that of bulk CeO_2 (3.19 eV for direct transition).[45] There are the decreased band gaps and the red-shift phenomenon of the absorption edge compared to bulk CeO_2, which can mainly be attributed to the abundance of their oxygen vacancies induced by their hierarchical structures and high surface area.[46,47] However, compared to CeO_2 nanoparticles (2.85eV) prepared by traditional precipitation methods, the increased band gap for the CeO_2 nanobundles demonstrates the occurrence of the blue-shift phenomenon. The blue-shift phenomenon can be dependent on smaller pore size of porosity structure and smaller grain size of primary particles for the nanobundles (Table S1) induced by quantum confinement effect.[44,45,48] CeO_2 nanobundles have a narrower band gap than nanowires and nanorods due to quantum confinement effect of smaller grain size and a possible shape effect prevailing over the size effect, respectively.[26]

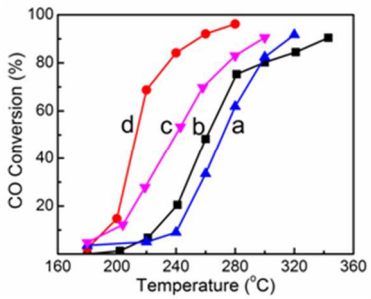

Fig.6 CO conversion as a function of temperature over CeO_2 materials. (a) Nanowires, (b) Nanoparticles, (c) Nanorods, (d) Nanobundles.

The catalytic oxidation of CO is an important catalytic process for many industrial applications, such as catalytic combustion for CO removal from vehicle exhaust, end-pipe gases, fuel cell and many other applications.[49,50] The CeO_2 materials are a typical catalyst for CO oxidation. Thus, CO oxidation is used to evaluate catalytic performance of CeO_2 materials with different morphologies. Fig.6 shows the catalytic performance of four CeO_2 nanostructure materials for CO oxidation as a function of reactive temperature. It can be seen that CeO_2 nanobundles exhibit higher CO conversion than other CeO_2 materials. The CO conversion of the CeO_2 nanobundles is over 84% at 240°C, whereas that of the CeO_2 nanorods, nanoparticles and nanowires is respectively 50%, 20% and 9% at the same reaction temperature. To be further comparable with the catalytic performance of these CeO_2 materials, the light-off temperature T_{50}, corresponding to 50% conversion of CO, is summarized in Table S1. From the calculated results, the nanobundles exhibit the lowest T_{50} value relative to other CeO_2 materials. We have further calculated the CO conversion rate of these CeO_2 nanostructure materials to compare their catalytic activities for CO oxidation. It is noticeable that CeO_2 nanobundles have the highest CO conversion rate at 240°C among all CeO_2 materials as shown in Table S1. Obviously, the CeO_2 nanobundles are provided with much higher catalytic activities for CO oxidation at 240°C than other CeO_2 material. Therefore, the catalytic results confirm that CeO_2 nanobundles have the superior catalytic activities for CO oxidation.

The characteristic results from TEM image and XRD pattern show that CeO_2 nanobundles expose the main crystal plane [111] and have similar lattice cell parameters with the CeO_2 nanorods and nanoparticles. However, the CeO_2 nanobundles have smaller primary grain size and much larger BET surface areas due to the existence of micropore and mesopore structure as shown in Table S1. This result demonstrates that there are more exposed surface oxygen and oxygen vacancy for the nanobundles due to the existence of more cerium and oxygen on the exposed surface of the nanobundles. For CO oxidation system, the participation of surface oxygen and oxygen vacancy in catalytic materials of metal oxides plays an important role and can directly influence catalytic properties of CO oxidation.[19,51,52] Thus, CeO_2 nanobundles can promote catalytic conversion of CO oxidation due to smaller grain size of their primary particles and much larger surface areas, compared with nanorods and nanoparticles. Although CeO_2 nanowires display the same exposed crystal plane and smaller grain size of their primary particles, they possess much lower BET surface areas and smaller lattice cell parameters which demonstrate their smaller lattice cell expansion and shorter Ce-O bond length to result in the fact that it is more difficult to escape surface oxygen and form oxygen vacancy on the surface of CeO_2 nanowires. Thus, CeO_2 nanowires exhibit much lower catalytic activity of CO oxidation than CeO_2 nanobundles.

H_2-TPR measurement can be used to reflect surface oxygen mobility revealed by the reducibility of CeO_2 samples and further verify the rationality of high catalytic activity of CO oxidation. TPR results in Fig.S5 confirm that CeO_2 nanobundles display the best redox behaviour among four CeO_2 samples. Thus, CeO_2 nanobundles are more easily reduced to provide surface oxygen species and promote oxygen mobility on their surface, relative to other CeO_2 materials. The better reducibility and higher oxygen mobility of surface oxygen on CeO_2 nanobundles is helpful to the occurrence of exhausted surface oxygen and the formation of oxygen vacancy, and lead to increase the catalytic performance for CO oxidation. Therefore, H_2-TPR measurement further demonstrates that CeO_2 nanobundles show the highest catalytic performance for CO oxidation among all CeO_2 samples.

4. Conclusions

In summary, CeO_2 nanobundles are successfully prepared by a facile carbonate-assisted formaldehyde hydrothermal route without templates or surfactants. It is crucial to form CeO_2 precursors with carbonate and formate during the employed hydrothermal system. It is noticeable that carbonate and ammonium ions play important roles in the morphology control of synthetic CeO_2 precursors and can promote the production of CeO_2 nanobundle precursors with carbonate and formate in the formaldehyde-assisted hydrothermal system.

Through a series of characterization methods, CeO_2 nanobundles prepared after calcining the corresponding precursors are revealed to possess hierarchical nanoarchitecture structure assembled by numerous nanorods with small diameter

Journal of Materials Chemistry A Accepted Manuscript

and porous feature with micropore and mesopore. It is also found that CeO_2 nanobundles with hierarchical and porous structure exhibit excellent physicochemical properties, such as larger lattice cell parameters, much larger surface areas and the best redox behaviour of surface oxygen on CeO_2 surface, relatively to CeO_2 nanords, nanowires and nanoparticles prepared by formaldehyde-assisted hydrothermal treatment and traditional precipitation methods. Thus, CeO_2 nanobundles with excellent physicochemical properties are used as active catalysts for CO oxidation to display superior catalytic activities.

Acknowledgments

This work was financially supported by the National Natural Science Foundation of China (No. 21073087 and No. 21101053), Natural Science Foundation of Anhui Province Science Research Project (No.1408085MB30), University Natural Science Research Project of Anhui Province (No. KJ2014A207) and Doctoral Scientific Research Funding of Hefei Normal University.

Notes and references

[a] *Department of Chemistry and Chemical Engineering, Hefei Normal University, Hefei, Anhui, 230601, PR China. E-mail:raorc123@163.com.*
[b] *Key Laboratory of Mesoscopic Chemistry, School of Chemistry and Chemical Engineering, Nanjing University, Nanjing ,Jiangsu, 210093, PR China. E-mail: zhangam@nju.edu.cn.*

† Electronic Supplementary Information (ESI) available. See DOI: 10.1039/b000000x/

1 G. Z. Shen, Y. Bando, C. J. Lee, J. Phys. Chem. B, 2005, **109**, 10578-10583;
2 B. Lim, M.J. Jiang, P.H.C. Camargo, E.C. Cho, J. Tao, X.M. Lu, Y.M. Zhu, Y.N. Xia, *Science*, 2009, **324**, 1302-1305.
3 B.-L. Su, C. Sanchez, X.-Y. Yang, *Insights into hierarchically structured porous materials: from nanoscience to catalysis, separation, optics, energy and life science,* Wiley-VCH Verlag & Co. KGaA, Boschstr, Weinheim, Germany, 2012, vol. 12, p. 69469.
4 J. Hu, L. Zhong, W. Song, L. Wan, *Adv. Mater.,* 2008, **20**, 2977-2982.
5 H. C. Zeng, *J. Mater. Chem.,* 2006, **16**, 649-662.
6 X. F. Zhou, S. Y. Chen, D. Y. Zhang, X. F. Guo, W. P. Ding, Y. Chen, *Langmuir,* 2006, **22**, 1383-1387.
7 J.K.H. Hui, P.D. Frischmann, C. Tso, C.A. Michal, M.J. MacLachlan, *Chem. Eur. J.,* 2010, **16**, 2453 -2460.
8 Y. X. Zhou, Q. Zhang, J. Y. Gong, S. H. Yu, *J. Phys. Chem. C,* 2008, **112**, 13383-13389.
9 B. Liu, H. C. Zeng, *J. Am. Chem. Soc.,* 2004, **126**, 8124-8125.
10 B. Liu, H. C. Zeng, *J. Am. Chem. Soc*., 2004, **126**, 16744-16746.
11 L. Z. Zhang, J. C. Yu, Z. Zheng, C. W. Leung, *Chem. Commun.,* 2005, **21**, 2683-2685.
12 A. M. Cao, J. S. Hu, H. P. Liang, W. G. Song, L. J. Wan, L. X. He, X. G. Gao, S. H. Xia, *J. Phys. Chem. B,* 2006, **110**, 15858-15863.
13 L.Y. Chen, Z. D. Zhang, W.Z. Wang, *J. Phys. Chem. C,* 2008, **112**, 4117-4123.
14 J. Wei, Z. Yang, Y. Yang, *CrystEngComm,* 2011, **13**, 2418-2424.
15 P. Wang, B. Bai, S. Hu, J. Zhuang, X. Wang. *J. Am. Chem. Soc.,* 2009, **131**, 16953-16960.
16 Y. Q. Qu, L. Liao, Y. J. Li, H. Zhang, Y. Huang, X. F. Duan, *Nano. Lett.*, 2009, **9**, 4539-4543.
17 S. Colodrero, A. Mihi, L. Haggman, M. Ocana, G. Boschloo, A. Hagfeldt and H. Miguez, *Adv. Mater*., 2009, **21**, 764-770.
18 A. Trovarelli, *Catal. Rev. Sci. Eng.,* 1996, **38**, 439-520.
19 A.Trovarelli, *Catalysis by Ceria and Related Materials,* Imperial College Press, London, 2002.
20 K. Zhou, X. Wang, X. Sun, Q. Peng, Y. Li, *J. Catal.,* 2005, **229**, 206-212.
21 H.X. Mai, L.D. Sun, Y.W. Zhang, R. Si, W. Feng, H.P. Zhang, H.C. Liu, C.H. Yan, *J. Phys. Chem. B*, 2005, **109**, 24380-24385.
22 X. Lu, D. Zheng, J. Gan, Z. Liu, C. Liang, P. Liu, Y. Tong, *J. Mater. Chem.,* 2010, **20**, 7118-7122.
23 Y. Zheng, K. Liu, H. Qiao, Y. Zhang, Y. Song, M. Yang, Y. Huang, N. Guo, Y. Jia, H. You, *CrystEngComm,* 2011, **13**, 1786-1788.
24 W.Q. Han, L. Wu, Y. Zhu, *J. Am. Chem. Soc.,* 2005, **127**, 12814-12815.
25 L. Gonzalez-Rovira, J.M. Sanchez-Amaya, M. Lopez-Haro, E.D. Rio, A.B. Hungria, P. Midgley, J.J. Calvino, S. Bernal, F.J. Botana, *Nano. Lett.,* 2009, **9**, 1395-1400.
26 R. Rao, Q. Zhang, H Liu, M. Yang, Q. Ling, A. Zhang. *CrystEngComm*., 2012, **14**, 5929-5936.
27 G. R. Li, D. L. Qu, Y. X. Tong, *Electrochem. Commun*., 2008, 10, 80-84.
28 C. Ho, J.C. Yu, T. Kwong, A.C. Mak, S. Lai, *Chem. Mater.,* 2005, **17**, 4514-4522.
29 Z. Guo, F. Du, G. Li, Z. Cui, *Cryst. Growth. Des*., 2008, **8**, 2674-2677.
30 G.Z. Chen, C.X. Xu, X.Y. Song, W. Zhao, Y. Ding, S.X. Sun, *Inorg. Chem.,* 2008, **47**, 723-728.
31 W. Liu, L. Feng, C. Zhang, H. Yang, J. Guo, X. Liu, X. Zhang , Y, Yang, *J. Mater. Chem. A*, 2013, **1**, 6942-6948.
32 G. J. Zhang, Z. R. Shen, M. Liu, C. H. Guo, P. C. Sun, Z. Y. Yuan, B. H. Li, D. T. Ding, T. H. Chen, *J. Phys. Chem. B,* 2006, **110**, 25782-25790.
33 T.Taniguchi, K. Katsumata, S. Omata, K. Okada, N. Matsushita, *Cryst. Growth Des.* 2011, **11**, 3754-3760.
34 Q.Yuan, H. Duan, L.Li, L.Sun, Y.Zhang, C.Yan, *J. Colloid. Interf. Sci*., 2009, **335**, 151-167.
35 R. B. Yu, L. Yan, P. Zheng, J. Chen and X. R. Xing, *J. Phys. Chem. C,* 2008, **112**, 19896-19900.
36 S. Uhm, Y. Yi, J. Lee, *Catal. Lett.*, 2010, **138**, 46-49.
37 E. Qi, B. Niu, S. Zhang, J. Wang, *Advanced Materials Research*, 2013, **624**, 88-93.
38 R. Rao, M. Yang, Q. Ling, Q. Zhang, H. Liu, A. Zhang, W. Chen, *Micropor. Mesopor. Mater.*, 2013, **169**, 81-87.
39 X. Li, J. Li, D. Huo, Z. Xiu, X. Sun, *J. Phys. Chem. C*, 2009, **113**, 1806-1811.
40 S. Yin, H. Hasegawa, D. Maeda, M. Ishitsuka, T. Sato, *J. Photochem. Photobio. A-Chem*., 2004, **163**, 1-8.
41 V.H. Schweer, H.Z. Seidel, *Z. Anorg. Allg. Chem.*, 1981, **477**, 196-204.
42 S.J. Gregg, K.S.W. Sing, *Adsorption, Surface Area and Porosity, Academic*, London, 1997.
43 S. A. C. Carabineiro, S. S. T. Bastos, J. J. M. Orfao, M. F. R. Pereira, J. J. Delgado, J. L. Figueiredo, *Appl. Catal., A*, 2010, **381**, 150-160.
44 S. Tsunekawa, T. Fukuda, *J. Appl. Phys*., 1999, **87**, 1318-1321.
45 Y. Zhang, R. Si, C. Liao, C. Yan, *J. Phys. Chem. B,* 2003, **107**, 10159-10167.
46 B.S. Zou, L.Z. Xiao, T. J. Li, J. L. Zhao, Z.Y. Lai, S.W. Gu, *Appl. Phys. Lett.,* 1991, **59,** 1826-1828.
47 X. Lu, D. Zheng, P. Zhang, C. Liang, P. Liu,Y. Tong, *Chem. Commun.,* 2010, **46**, 7721–7723.
48 D. Xu, G. Guo, L. Gui, Y. Tang, B.R. Zhang, G.G. Qin, *J. Phys. Chem. B,* 1999, **103**, 5468-5471.
49 J.N. Armor, *Appl. Catal. A,* 1999, **176**, 159-176.
50 J.T. Kummer, *J. Phys. Chem.,* 1986, **90**, 4747-4752.
51 D.R. Mullins, S.H. Overbury, *J. Catal.,* 1999, **188**, 340-345.
52 V. Shapovalov, H. Metiu, *J. Catal.,* 2007, **245**, 205-214.

Journal of Materials Chemistry A Accepted Manuscript

This journal is © The Royal Society of Chemistry [year]

A facile synthesis for hierarchical porous CeO_2 nanobundles and their superior catalytic performance for CO oxidation

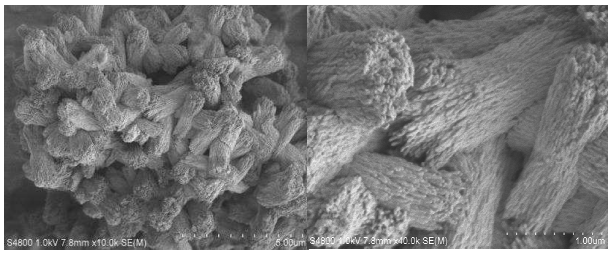

Porous CeO_2 nanobundles with hierarchical nanoarchitecture show much better catalytic activities for CO oxidation than CeO_2 nanorods, nanowires and nanoparticles.

Journal of Materials Chemistry A Accepted Manuscript